Precambrian Research 403 (2024) 107306

Contents lists available at ScienceDirect

Precambrian Research

journal homepage: www.elsevier.com/locate/precamres

Deep magmatic staging chambers for crustal layered mafic intrusions: An example from the Bushveld Complex of southern Africa

Janine Cole [a,*], Carol Ann Finn [b], Susan Jane Webb [c]

[a] Council for Geoscience, Private Bag X112, Pretoria 0001, South Africa
[b] U.S. Geological Survey, MS964, Denver Federal Center, Denver, CO 80225, USA
[c] School of Geosciences, University of the Witwatersrand, Private Bag 3, WITS 2050, South Africa

A R T I C L E I N F O

Keywords:
Bushveld Complex
Geophysical model
Staging chamber

A B S T R A C T

The deep mafic magmatic staging chambers of layered mafic intrusions have been conjectured but not imaged. Their existence has long been postulated from geochemical models which require multiple magma injections from staging chambers to account for their multi-scale igneous layering and variations in sources and degrees of crustal contamination. For the Bushveld Complex of southern Africa, the world's largest layered mafic intrusion, seismic receiver functions identify a diffuse crust-mantle transition beneath the Complex that suggests high velocity lower crust and/or uppermost lithospheric mantle. Here we present 3D gravity modelling of the Bushveld Complex that includes dense material at the crust-mantle boundary, imaging for the first time, remnants of magma staging chambers. They underlie the whole Bushveld Complex and extend westwards to the Molopo Farms Complex in Botswana. Feeders to the Bushveld Complex coincide with intersections of major faults like the Thabazimbi-Murchison Lineament and Sugarbush Fault with the staging chamber. This identification of magmatic staging chambers beneath the Bushveld relates to similar geophysically imaged lower crustal features beneath the Duluth and Stillwater Complexes. Comparison of seismic and gravity data with geochemical models from other complexes aid in development of models for the magmatic architecture of layered mafic intrusions in general.

1. Introduction

Magmatic systems consisting of transcrustal magma chambers effectively explain the formation of volcanic arcs (Marsh, 2015; Cashman et al., 2017; Sparks et al., 2019). Similar models for layered mafic intrusions are not widely accepted (Latypov et al., 2022b, 2022a). Based on geochemical evidence, deep-seated crustal magma chambers explain compositional changes in layered intrusions globally (Hanski et al., 2001; Owen-Smith and Ashwal, 2015; Jenkins et al., 2021), including the Bushveld Complex, the world's largest layered igneous intrusion (Ashwal et al., 2005; Eales and Costin, 2012; Maier et al., 2013; McDonald and Holwell, 2007; Prevec et al., 2005; Roelofse and Ashwal, 2012; Wilson, 2012; Yao et al., 2021). However, these deep seated chambers have not been imaged. Here, we combine seismic, geologic and gravity data into a model that image, for the first time, a staging chamber beneath the Bushveld Complex.

The Bushveld Complex crops out in four lobes in northern South Africa, with a covered fifth lobe in the southeast (Fig. 1). It consists of the mafic/ultramafic Rustenburg Layered Suite (RLS, dated at 2055.91 $\pm$ 0.26 Ma) and the contemporaneous acidic Rashoop Granophyre and Lebowa Granite Suite (Scoates et al., 2021; Skursch et al., 2022; Mungall et al., 2016; Zeh et al., 2015). The RLS is divided into five zones, each of which displays substantial geochemical cyclic layering. The exception to this is a thick succession of norite and gabbronorite of the Main Zone. An extra layered unit, the Basal Ultramafic Sequence, was recently identified at the base of the RLS in the eastern lobe (Wilson, 2015). There appears to be consensus that multiple magma injections account for most of the layering, although the number of magma pulses and compositions of parental magmas and their sources are still hotly debated (Cawthorn, 2007; Eales and Costin, 2012; Kruger, 2005; Tegner et al., 2006; Wilson, 2012, 2015; Yao et al., 2021). The Bushveld Complex in Botswana comprises the Molopo Farms Complex a mafic - ultramafic layered intrusion dated at 2054 $\pm$ 5 Ma (Beukes et al., 2019) and the Moshaneng Complex composed of mafic and felsic rocks with the latter dated at 2054 $\pm$ 2 Ma[59]. (Fig. 1).

Large ENE-striking faults coincide with boundaries in the Bushveld

* Corresponding author.
E-mail addresses: jcole@geoscience.org.za (J. Cole), cfinn@usgs.gov (C.A. Finn), susan.webb@wits.ac.za (S. Jane Webb).

https://doi.org/10.1016/j.precamres.2024.107306
Received 7 September 2023; Received in revised form 23 December 2023; Accepted 22 January 2024
Available online 7 February 2024

Complex (Fig. 1). RLS rocks of the northern lobe crop out south of the Palala Shear Zone which forms the boundary between the Kaapvaal Craton the Limpopo Mobile Belt to the north which separates the Kaapvaal and Zimbabwe Cratons that collided roughly 2.6 Ga (Geng et al., 2014). The Palala Shear Zone underwent a phase of strike-slip faulting between the time of the Bushveld Complex intrusion and later sedimentary deposition between 1.95 and 1.85 Ga (Schaller et al., 1999). The Thabazimbi-Murchison Lineament (TML) forms a lithospheric boundary between the northern and western and eastern lobes, extending to the mantle and has been episodically reactivated since at least 2.96 Ga (Good & De Wit, 1997). Because the TML represents a zone of weakness, it localized feeders to the Bushveld Complex (Du Plessis and Walraven, 1990; Good and De Wit, 1997; Kruger, 2005; Clarke et al., 2009; Finn et al., 2015; Özaydın et al., 2022). The Sugarbush Fault along the southern margin of the south-eastern lobe is not well understood and has been described as a left-lateral wrench fault, a normal fault and a combination of normal and sinistral faulting, and pre-dates the Bushveld (Dankert and Hein, 2010). The Inyoka Fault represents a suture zone between Archaean blocks that amalgamated ~3 Ga (De Wit et al., 1992) and crops out in the Barberton Greenstone Belt roughly 100 km to the east.

Gravity modelling shows that the lobes are interconnected at depth (Webb et al., 2004; Cole et al., 2014; Finn et al., 2015). Seismic receiver function data (Fouch et al., 2004) confirmed thick crust underneath the Bushveld Complex and that the crust-mantle transition underneath the Bushveld Complex was less defined than under the surrounding undisturbed Kaapvaal Craton (Nguuri et al., 2001; Nair et al., 2006; Kgaswane et al., 2009, 2012; Youssof et al., 2013; Delph and Porter, 2015). Here (Nguuri et al., 2001; Nair et al., 2006; Delph and Porter, 2015) and in other parts of Southern Africa (e.g. under the Central Zone of the Limpopo Mobile Belt (Gore et al., 2009; Stankiewicz and De Wit, 2013), under the Okwa/Magondi terranes to the west of the Limpopo Mobile Belt and Zimbabwe Craton (Nguuri et al., 2001; Mapeo et al., 2004) (see inset in Fig. 1) and under the Namaqua Metamorphic Province (Durrheim and Green, 1992; Stankiewicz and De Wit, 2013), diffuse Moho has generally been only attributed to mafic underplating of indeterminate age and emplacement process, not as staging chambers.

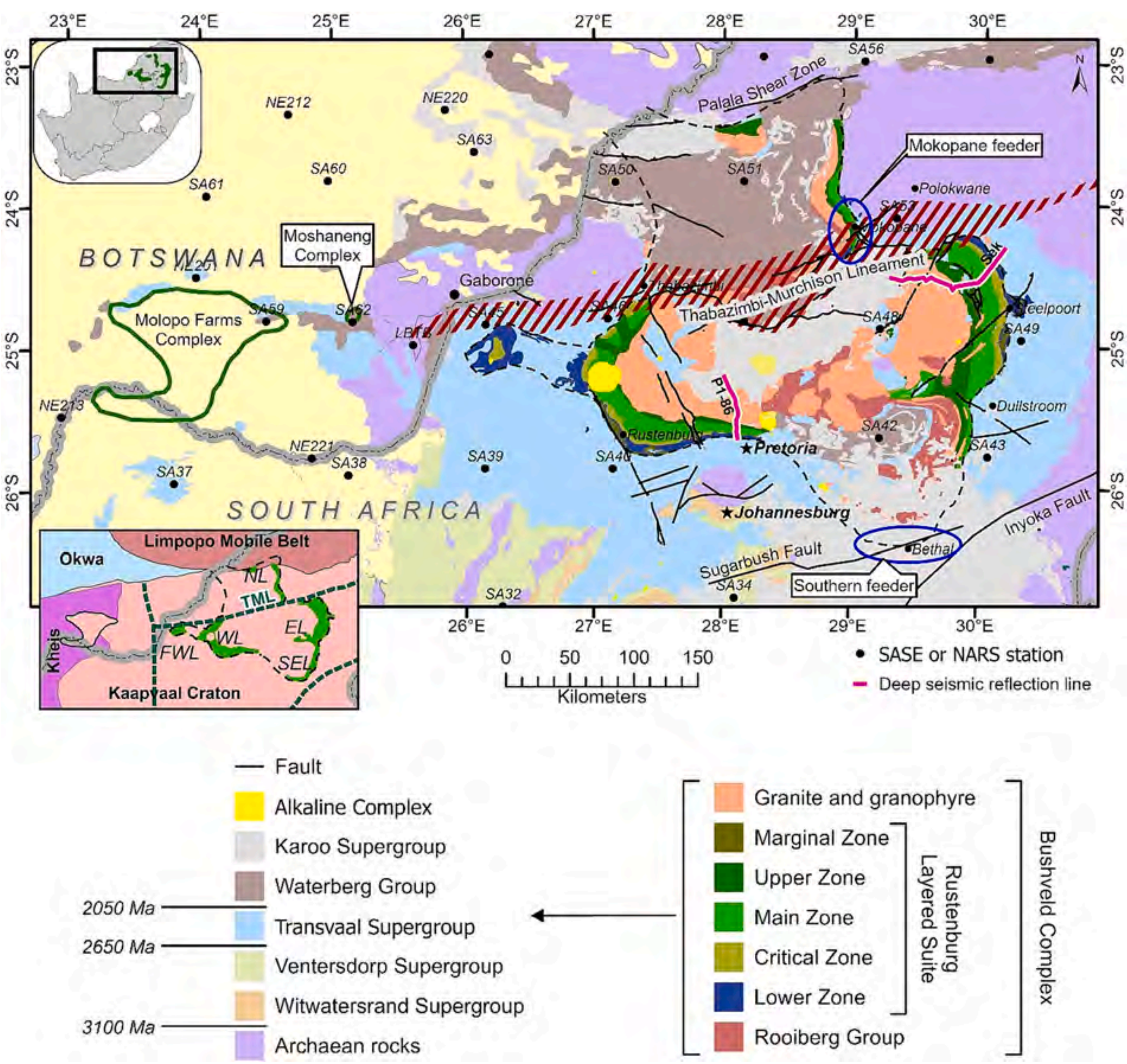

Fig. 1. Simplified geological map of the Bushveld Complex. The dashed black line shows the extent inferred from geophysical data. Blue ellipses indicate feeders inferred from gravity data. The dark red hatching is the Thabazimbi Murchison Lineament. Lower left inset: NL – Northern lobe, EL – Eastern lobe, SEL – South-eastern lobe, WL – Western lobe, FWL – Far western lobe. SASE (Southern African Seismic Experiment data (Fouch et al., 2004). NARS (Network of Autonomously Recording Seismographs) (Fadel et al., 2018).

2. Data and methods

2.1. Gravity data

Regional gravity data with a resolution of roughly one measurement every 14 km^2 cover the Bushveld Complex. The data were collected during the 1970s to the 1990s using LaCoste and Romberg gravimeters. Elevations were determined using micro-barometers. Bouguer anomaly values were calculated assuming a mean density of 2670 kg/m^3. The measurements were tied to the International Gravity Standardisation Net values (Morelli et al., 1997) and referred to the gravity formula based on the 1980 geodetic reference system (Moritz, 1992). The maximum error (including reading, positional and elevation inaccuracies) in the Bouguer anomaly value was estimated to be within 2 mgal (Stettler et al., 2000). The Botswana gravity data were collected during the 1970 s and 1990 s at an average resolution of 7.5 km (Chisenga et al., 2020). The gravity data were gridded at a 2 km cell size. The Bouguer anomaly map (Fig. 2a) was produced using the standard latitude, free-air correction and Bouguer slab correction.

2.2. Broadband seismic data (SASE and NARS)

Between 1997 and 1999 an array of three-component seismometers was deployed across Southern Africa to form the Southern African Seismic Experiment (SASE). Data were recorded at a total of 79 temporary stations, spaced ~ 100 km apart. and supplemented by data from three permanent broadband stations (Fouch et al., 2004). Sixteen of the stations were located on or in the vicinity of the Bushveld Complex (Fig. 1). The Network of Autonomously Recording Seismographs in Botswana (NARS-Botswana) consisted of 21 broadband seismic stations deployed between November 2013 and February 2018 (Fig. 1) (Fadel et al., 2018). The stations were spaced roughly 150 – 200 km apart.

2.3. Gravity modelling

GM-SYS 3D is a 3D gravity and magnetic modelling package for surface-oriented models. A model is defined by a number of stacked surface grids with density distributions specified for the layer below each surface. Calculations are performed in the wave number domain (Parker, 1972).

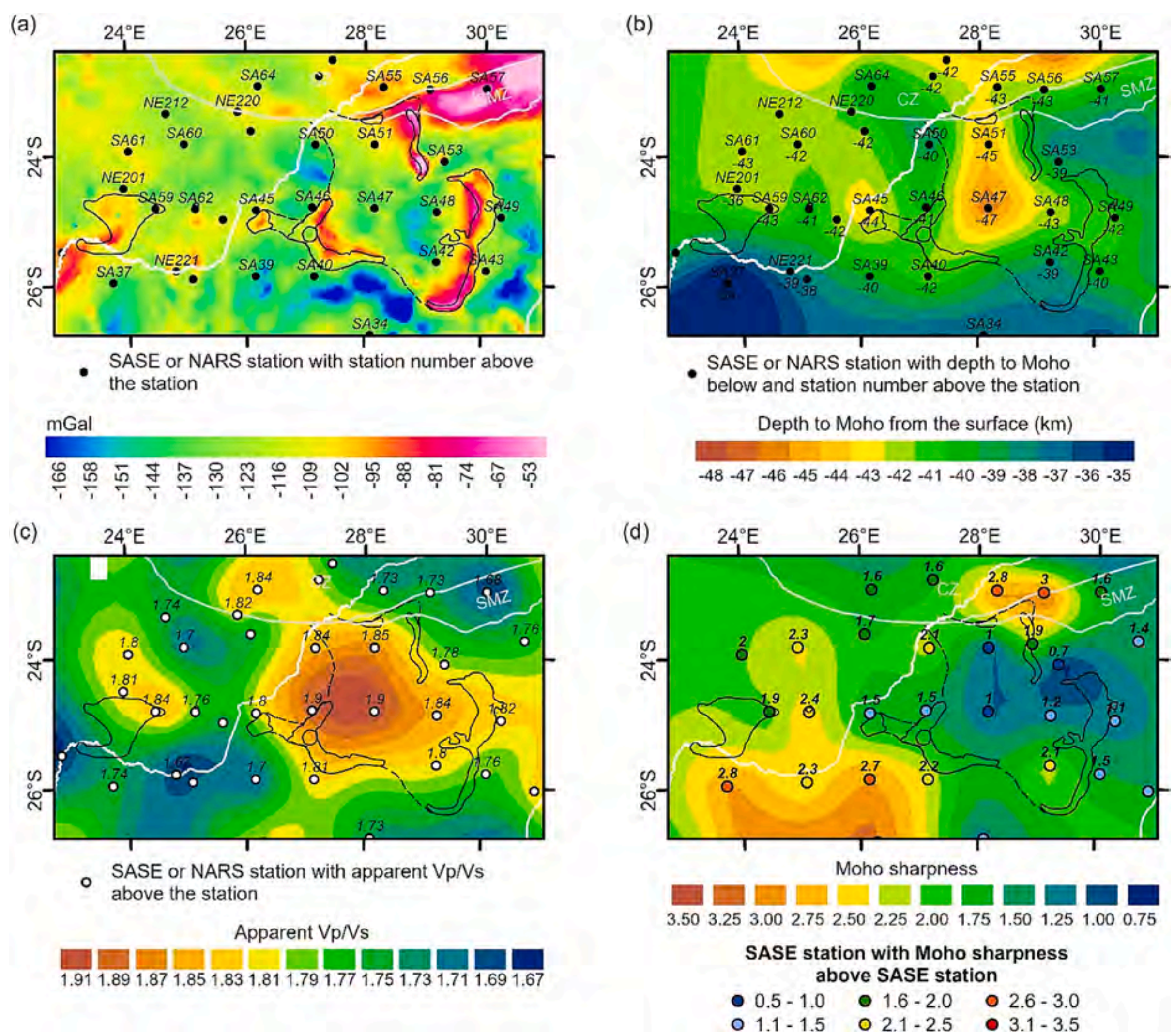

Fig. 2. Gravity data and results from seismic receiver function studies. The Northern Marginal Zone (NMZ), Central Zone (CZ) and Southern Marginal Zone (SMZ) of the Limpopo Belt are outlined (Kgaswane et al., 2009). (a) Bouguer anomaly map; (b) Average crustal thickness of five different models (Nguuri et al., 2001; Nair et al., 2006; Kgaswane et al., 2009, 2012; Youssof et al., 2013; Delph and Porter, 2015); (c) Apparent V_p/V_s calculated by Delph and Porter (2015); (d) Moho sharpness determined by Youssof et al (2013). The Moho sharpness quantifies the quality of the P to S conversions. Higher values indicate sharper Moho.

2.4. Crust-mantle transition

Seismic receiver function studies show weak P to S wave conversions at the crust-mantle interface underneath the Bushveld Complex (Nguuri et al., 2001; Nair et al., 2006; Youssof et al., 2013; Delph and Porter, 2015). These studies used H-k stacking (Zhu and Kanamori, 2000) to determine the crustal thickness (H) and V_p/V_s (k) (where V_p is the P-wave velocity and V_s is the S-wave velocity) (Fig. 2b,c) and provide valuable information regarding crustal composition (for example, a high ratio reflect decreasing silica content as for mafic rocks) (Zandt and Ammon, 1995). V_p/V_s higher than 1.77 (the average crustal ratio) generally indicates more mafic material (Christensen, 1996; Delph and Porter, 2015). Diffuse crust-mantle transitions can explain weak conversions. Magmatic underplating can cause these diffuse transitions or, in the case of the Limpopo Belt, high metamorphic grade/velocity crust related to shortening and crustal thickening during the collision of the Kaapvaal and Zimbabwe cratons in the Archean (James et al., 2003). Another explanation may be the lower velocity contrast between the lower crust and a Mg-depleted upper mantle beneath the Bushveld Complex. Low seismic velocities in the mantle under the Bushveld Complex may result from an increase in Fe content due to refertilisation (James et al., 2001). The Moho sharpness factor, calculated by comparing the Pds (P to S conversion at a depth d) phase amplitude at a receiver station to the average Pds amplitude for the entire SASE study area, is generally low (<1.5) over the Bushveld Complex also indicating a diffuse Moho (Youssof et al., 2013) (Fig. 2d). Application of a Gaussian-weighting common conversion point stacking for each receiver function to obtain better resolution variations in spatial amplitude also encountered weak conversions for most of the Bushveld Complex (Delph and Porter, 2015). In these instances H and k values that gave the best stacking amplitudes were selected manually and not through an automated iterative process.

The seismic receiver function studies (Fig. 2b-d) show the thickest, most diffuse crust-mantle transitions under the centre of the Bushveld Complex, extending to the far western lobe, and under the northern lobe. The Molopo Farms Complex in the west (SA59) also correlates with more diffuse Moho. The stations south of the western and south-eastern lobes (SA 40 to SA 42) generally record high amplitude P to S conversions.

The gradational transition underneath the Bushveld Complex is generally attributed to mafic underplating (Nguuri et al., 2001; Youssof et al., 2013) and mafic lower crust (Kgaswane et al., 2009, 2012; Delph and Porter, 2015). Another possible explanation for underplating may relate to the Karoo magmatic event that saw the eruption of basaltic lava and the intrusion of dolerite sills throughout southern Africa and Antarctica during the break-up of Gondwana around 180 Ma (Jourdan et al., 2005). However, silicic crust ($V_p/V_s < 1.77$, Delph and Porter, 2015) and a sharp Moho (>2.0, Youssof et al., 2013) correlate with the Karoo Dolerite Suite. Another possibility is that the Archean lower crust was mafic prior to the intrusion of the Bushveld Complex, but results from a dense seismic array near Kimberley, outside of the Bushveld Complex, shows a lower crust of intermediate composition (Niu and James, 2002). Similarly, seismic refraction studies over the Witwatersrand Basin south of the Bushveld Complex produced V_p of 6.5–6.8 km/s for the lower crust, described as felsic granulite (Durrheim and Green, 1992).

2.5. Gravity inversion modelling

Refertilization increased the density of the upper mantle. To maintain the diffuse velocity contrast at the Moho higher densities are necessary at the base of the lower crust. For modelling purposes we averaged five different crustal thickness models (Nguuri et al., 2001; Nair et al., 2006; Kgaswane et al., 2009, 2012; Youssof et al., 2013; Delph and Porter, 2015) as done for the Northern Lobe (Finn et al., 2015).The thicknesses vary in places but uncertainties in crustal thicknesses in areas with diffuse Moho are ~ 5 km (Kgaswane et al., 2009). The maximum RLS thickness was conservatively limited to 10 km, although geologic outcrop, drilling (Teigler and Eales, 1996; Ashwal et al., 2005; Roelofse and Ashwal, 2012) and seismic reflection data (Odgers and Du Plessis, 1993; Odgers et al., 1993; Campbell, 2011) show the intrusion to be roughly 7 km thick. These geological, borehole and seismic data sets constrained the model of the Bushveld Complex. Crustal thicknesses derived from the NARS-Botswana (Fadel et al., 2018) supplemented the SASE data to allow for a westward extension of the modelling.

Densities for the lower crust were derived from shear wave velocities (Kgaswane et al., 2009, 2012). The velocities (4.0 to 4.3 km/s) translate to densities between 3145 kg/m^3 and 3360 kg/m^3 (using the empirical equation of Christensen and Stanley (2003), with an average of 3250 kg/m^3. Increasing the density to 3340 – 3350 kg/m^3 (Artemieva and Vinnik, 2016) did not change the inversion result, and a mantle density of 3330 kg/m^3 was used for the mantle underneath the Bushveld Complex. SASE results also guided the densities used for the lower crust and mantle. Detailed seismic tomography work on an undisturbed part of the Kaapvaal Craton in South Africa revealed a lower crust with a density of 2860 kg/m^3 overlying a dense mantle (3300 kg/m^3) (Niu and James, 2002).

To test whether dense material can be modelled underneath the Bushveld Complex, we used a commercial software package (GMSys3D) to invert the gravity data (Fig. 2a) to 3D models of density (Parker, 1972) with and without dense lower crustal material. Both starting models consisted of a 1 km thick layer of cover material (2500 kg/m^3), an 8 km layer representing the RLS (3010 kg/m^3), and the Moho (3250 kg/m^3) defined by the average thickness of the five different crustal thickness models (Nair et al., 2006; Kgaswane et al., 2009, 2012; Youssof et al., 2013; Delph and Porter, 2015). The middle crust was given a density of 2700 kg/m^3 (Webb et al., 2004). The horizontal and vertical resolutions of the model were both 5 km. In the first model, dense lower crust was not added. The top of the RLS was allowed to vary by 500 m but the variations of the bottom were unrestricted. The resulting RLS thickness ranged between roughly 7 km and 20 km, with thicknesses above 19 km for more than half of the Bushveld Complex (Fig. 3). Borehole and seismic data refute this excessive thickness.

In the second model one dense (3020 kg/m^3) lower crustal layer with a starting thickness of 24 km was added above the Moho because the seismic identification of high velocities is most reliable for the lower crust. The top of this layer was allowed to vary, and the RLS thickness was constrained to less than 10 km away from possible feeders (Fig. 4a). Inversion resulted in a dense lower crust under the whole Bushveld Complex (Fig. 4b). Under the western and northern lobes the thickness varied between ~14 km and 22 km (Profiles 1, 3 and 4 in Figs. 4 and 5), while under the eastern lobe it was ~14 km to 16 km thick (Profile 2 in Figs. 4 and 5), The layer was thickest under the TML between the northern and western lobes (Fig. 3b). Including a mid crustal (~15 km depth) dense layer while reducing the thickness of the lower crustal layer and/or the Bushveld Complex is consistent with, but not required by, the gravity and seismic data. We focus on interpretation of the lower crustal body.

Depths to the top of the dense lower crust were extracted at the SASE stations and compared to depths where shear wave velocities were greater than 4.0 km/s (defined as the threshold for dense lower crust by Kgaswane et al., 2012) (Fig. 5e). The velocity models had a depth resolution of 5 km. Six of the inversion model depths fell within 5 km of the velocity model depths. For the rest of the stations the inversion model depths were shallower than the velocity model depths.

The seismic velocity models are inversion models themselves with uncertainties of 0.1 to 0.2 km/s (Kgaswane et al., 2012). When comparing velocity depths where Vs > 3.9 km/s with the inversion results, seven of the stations had depths within 5 km and SA51 was just outside of 5 km (Fig. 5f). The gravity inversion and seismic velocity models yielded comparable results within the resolutions and

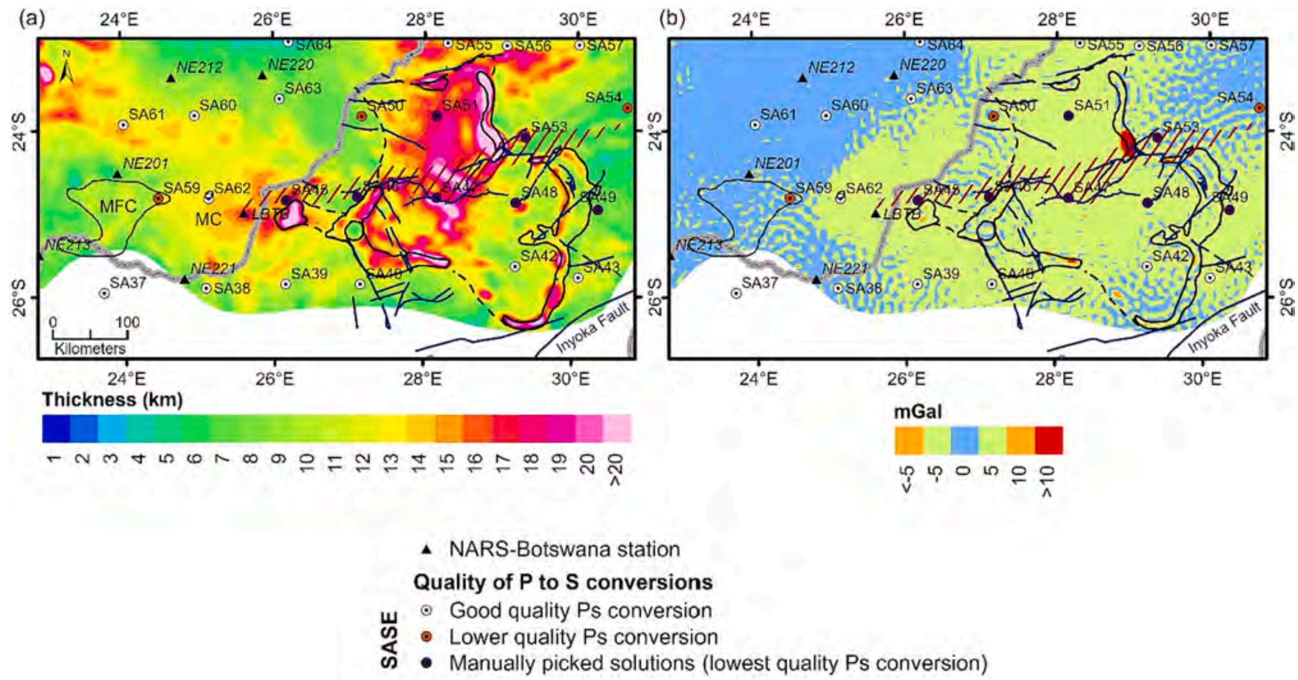

Fig. 3. (a) Thickness of the RLS from the inversion without dense lower crust included in the model; (b) Residual gravity.

uncertainties of the models.

3. Discussion

The regional gravity modelling requires dense material in the crust below the RLS. The thickness of this layer depends on its density and the thickness and density of the RLS in the upper crust. As the maximum thickness of the RLS is constrained to ~ 7–8 km by seismic reflection and borehole data (Cawthorn and Walraven, 1998) and its density has been determined from laboratory and downhole measurements (Cole et al., 2021), the deeper-seated dense material is required to model the observed gravity data. Non-uniqueness in potential field modelling means that other models can fit the data, but high seismic velocities, and therefore high densities, are present in the lower crust, thereby constraining our model.

The dense lower crust spatially correlates with the large ENE-striking faults, (Fig. 4b). Although co-location does not imply interaction between the faults and the dense material it does present the possibility of at least some faults tapping into a deeper-seated source. Correlation between two modelled feeders and two of the faults makes this possibility more enticing.

The Mokopane feeder coincides with the intersection of north-trending faults in the northern lobe, and NE and ENE striking faults that form part of the TML (Finn et al., 2015). The inversion result shows the feeder coinciding with thicker dense lower crust, raising the possibility that they could have been connected at some stage. This may actually still be the case, but the resolution of the model is too coarse to constrain such a scenario (Fig. 5d). The dense lower crust is thickest under the central part of the TML and thins to the east and west but becomes thicker again along the northern boundary of the far western lobe (Fig. 4b). The TML has been described as a large-scale relay structure at the time of the Bushveld Complex intrusion (Good and De Wit, 1997) [55]. The structural complexity of relay structures makes them ideal pathways for fluids, including magmas (Dankert and Hein, 2010). Although our model is too regional to show complexity in the TML, it coincides with thick upper and lower crustal dense material (Fig. 4). Inverse modelling also showed dense material potentially related to feeders (Finn et al., 2015) caught up in the TML.

The proposed southern feeder was best forward modelled with a conduit extending down to 20 km (Cole et al., 2021). The inversion results show a thinner feeder, ~5.5 km thick but underlain by thick mafic lower crust, suggesting a possible trade-off between its thickness and the lower crustal thickness (Fig. 4). Boreholes intersected only Upper and Lower Zone rocks and on the basis of this it was interpreted as a separate lobe with its own feeder (Buchanan, 1975). Later, Sr-isotope studies of magma compositions suggested that a feeder at the south-eastern lobe was the source of the Upper Zone in the south-eastern, western and eastern lobes (Kruger, 2005). The Sugarbush Fault has never been explicitly mentioned as a possible feeder zone for the Bushveld Complex, however, its position along the southern margin of the south-eastern lobe where both a feeder and staging chamber have been modelled makes it a strong candidate. It was active prior to the intrusion of the Bushveld Complex, but its tectonic history has not been studied (Dankert and Hein, 2010) and it is also unknown whether the fault extends down to the mantle. The Inyoka Fault represents a suture zone of two Archaean blocks and likely extends to the mantle (Fig. 1). However, its exact position is uncertain and the correlation with the modelled staging chamber may be fortuitous.

Thickness of the dense lower crustal layer shows strong agreement with areas of deep mafic material above a diffuse Moho (Fig. 2c, d). The thickest part of the dense lower crust corresponds toto diffuse Moho (Youssof et al., 2013), high Vp/Vs is high, indicating mafic material (Delph and Porter, 2015) and the thickest crust (Fig. 2b). Under the outcropping eastern and western lobes, the dense lower crustal layer is thinner. Under the Far Western lobe it becomes thicker over deeper Moho. The thick mafic lower crust extends even further west to the Molopo Farms Complex (MFC) where the NARS data also showed a high Vp/Vs ratio of 1.81 at station NE 201 just north of the MFC which corroborates the presence of mafic material at depth (Fig. 2c). The dense material therefore extends ~ 700 km in an east–west direction and ~ 350 km in a north–south direction under the Bushveld Complex.

The link between layered igneous intrusions of Bushveld age and a thick layer of dense lower crustal material is clear. The cause of the dense material has in the past been described as mafic underplating with no relation to shallower magmatism (Nguuri et al., 2001; Youssof et al., 2013). We propose that it reflects the remnants of a deep-seated mush

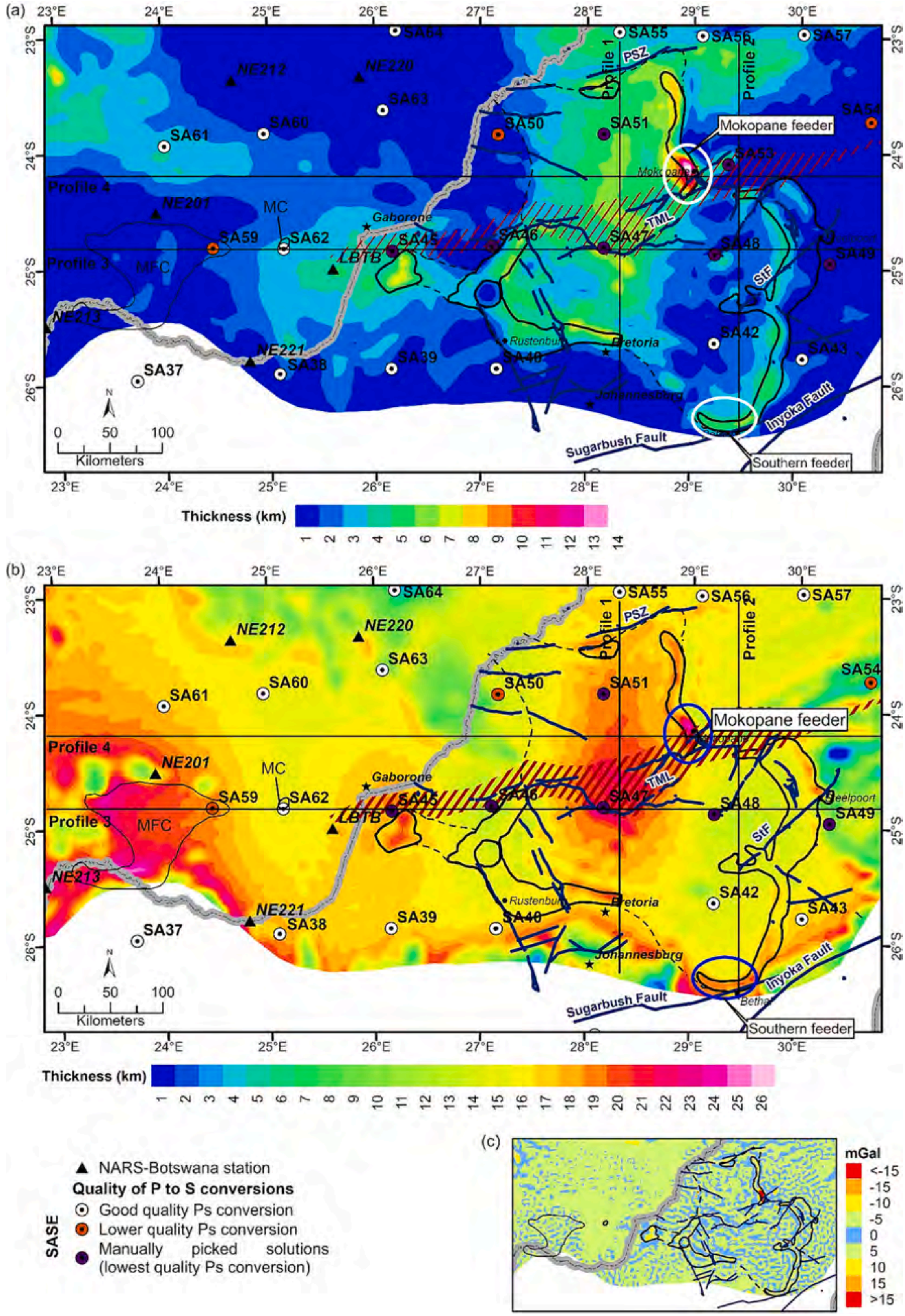

Fig. 4. (a) Thickness of the RLS from the inversion; (b) Thickness of the dense lower crust resulting from inversion; (c) Residual gravity. Thick blue lines are known faults. The cross-hatched area indicates the TML; PSZ – Palala Shear Zone; StF – Steelpoort Fault; TML – Thabazimbi-Murchison Lineament; MFC – Molopo Farms Complex; MC – Moshaneng Complex. Inversion results extracted along profile 1 to 4 are shown in Fig. 5.

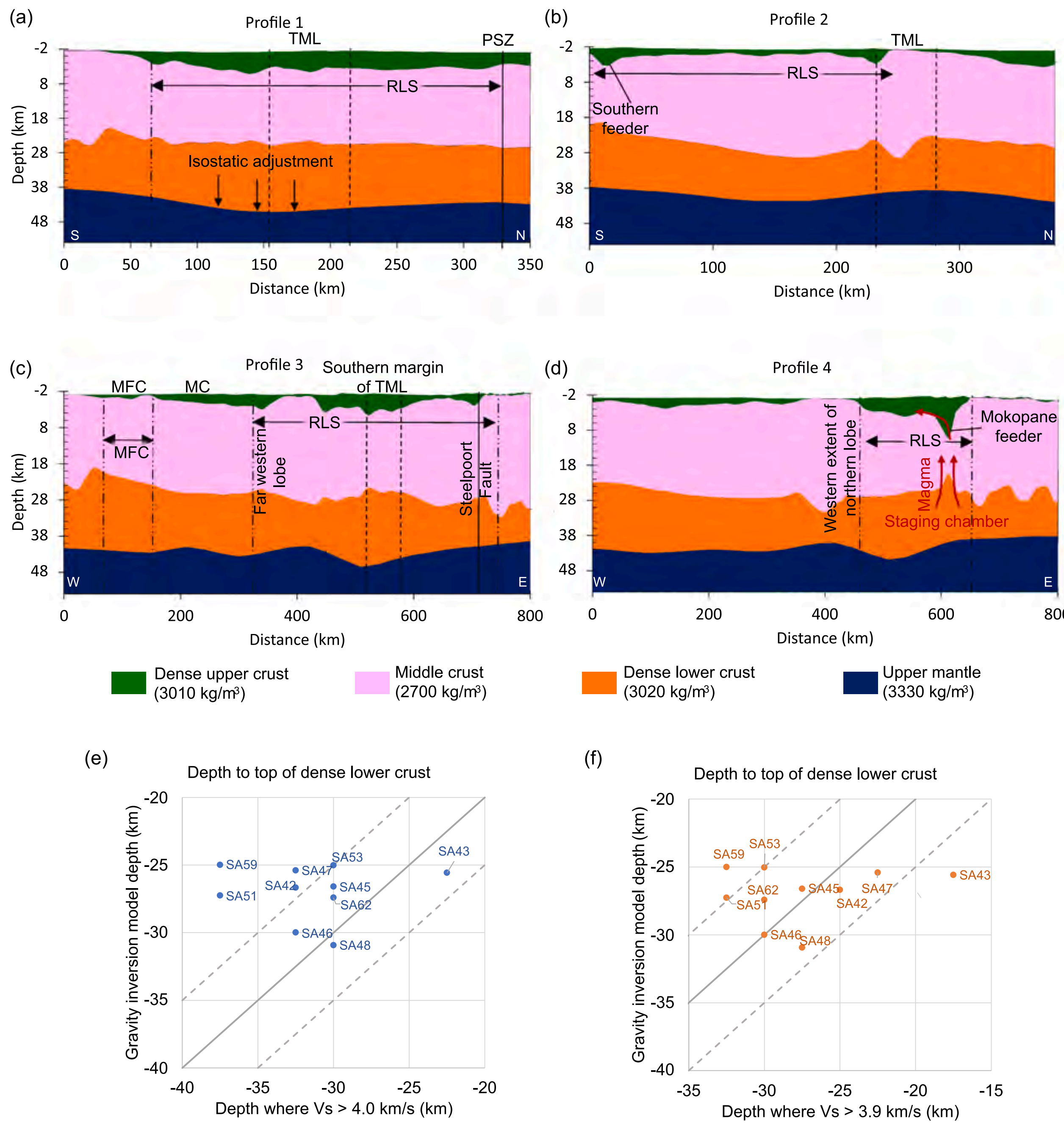

Fig. 5. Profiles extracted from the inversion results and comparisons with shear wave seismic velocity models. Profile localities are shown in Fig. 4. (a) – (d) Dashed lines designate the rough extent of the TML, dash-dot-dot-dash lines indicate estimated lateral extents of the RLS and MFC, solid lines are faults from the geological map and extended vertically down for illustration purposes. RLS – Rustenburg Layered Suite; MFC- Molopo Farms Complex; MC – Moshaneng Complex; TML – Thabazimbi-Murchison-Lineaments; PSZ – Palala Shear Zone; (e) Depths to the top of the dense lower crust compared to the depth of a high Vs layer in the lower crust (Vs > 4.0 km/s) The grey line is a 1:1 relation, dashed grey lines show 5 km on either side of the 1:1 relation; (f) Depths to the top of the dense lower crust compared to the depth of a high Vs layer in the lower crust (Vs > 3.9 km/s).

zone inferred from thermodynamic modelling that fed the RLS (e.g. Yao et al., 2021). It is not possible to distinguish between remnants of staging chambers and magmatic underplating from geophysical data alone, but the presence of deeper-seated staging chambers explains geochemical complexities in the RLS such as the chromium paradox. The extensive chromite layers in the Lower Critical Zone require parental magmas more enriched in chromium than is possible for the presumed parent magmas (Eales and Costin, 2012). Mixing of komatiitic and crustal melts in a staging chamber from which chromite-rich crystal slurries were injected into the shallower intrusion can explain the high chromite content (Eales and Costin, 2012) as can the injection of crystal mushes enriched in chromite through batch crystallisation (Yao et al.,2021). The remaining ultramafic material in the staging chamber causes the dense lower crustal material. Crystal mushes with variable amounts of crustal contamination in a lower crustal staging chamber were also proposed to explain isotopically heterogeneous plagioclase in the Main Zone (Roelofse et al., 2015). Thermodynamic models of middle crust assimilating with mantle melts in a staging chamber at ~ 17 km depth (pressure of 0.45 Ga) explain the composition of the gabbronoritic part of the Lower Main Zone and Upper Critical Zone. An estimated 90–97 % of the solids crystallized at this depth, potentially leaving high density material at mid-lower crustal depths. To model the generation of the Upper and

Upper Main Zone magmas, an assimilation-fractional crystallization model of lower crust at a pressure of 1 GPa would have left even more high-density solids in the lower crust (Yao et al., 2021).

The relation between staging chambers and large structures has been observed elsewhere. High-density 3D magnetotelluric data imaged a lower-crustal mush zone from which melt ascends via pre-existing structures beneath Mt. St. Helens (Bedrosian et al., 2018). Another modern analogue is the Hawaiian volcanic system where microseismicity revealed the link between staging chambers (the Pahala sill complex) at 36–43 km depth and the 2020 and 2021 eruption at Kilauea (Wilding et al., 2022). Thus, the correlation of large fault structures and modelled feeders with the dense material in the lower crust beneath the Bushveld Complex and MFC, combined with geochemical arguments for the existence of staging chambers from which the RLS was fed makes for a compelling argument that the deep-seated dense material under the Bushveld and Molopo Farms complexes are remnants of staging chambers. Large faults that predate the intrusion of the Bushveld Complex and intersect with the modelled staging chamber, form zones of weakness ideally located to tap a magma staging chamber that formed at the Moho. The exact thickness, and therefore shape of the staging chamber cannot be constrained, but the seismic and gravity data show that they extend well into the lower crust.

Our results have implications for linking the sources of magmatism based on geochemistry in other intrusions with dense lower crust (e.g., Alghamdi et al., 2018; Finn et al., 2020). Imaging the location of magma staging chambers is important for understanding the genesis of these economically important intrusions which is hotly debated, especially in the Bushveld (Latypov and Chistyakova, 2022; Latypov et al., 2022a,b; Maghdour-Mashhour et al., 2021; Mungall et al., 2016; Yao et al., 2021). Regional seismic networks image high velocities in the base of the crust beneath the Duluth Complex where gravity modelling requires high densities conjectured to relate to a staging chamber (Peterson and Bedrosian, 2023). High seismic velocities (Schulte-Pelkum et al., 2017) and densities near the Stillwater Complex (Finn et al., 2020) may indicate a staging chamber that was dismembered from the Complex during faulting. High density seismic networks would help image lower crustal staging chambers beneath layered mafic intrusions, constraining gravity modelling in other regions.

CRediT authorship contribution statement

Janine Cole: Conceptualization, Data curation, Investigation, Methodology, Visualization, Writing – original draft, Writing – review & editing. **Carol Ann Finn:** Conceptualization, Investigation, Methodology, Visualization, Writing – review & editing. **Susan Jane Webb:** Conceptualization, Methodology, Writing – review & editing.

Declaration of competing interest

The authors declare that they have no known competing financial interests or personal relationships that could have appeared to influence the work reported in this paper.

Data availability

Gravity, petrophysical and geological data collected by the Council for Geoscience are available at https://maps.geocience.org.za. OasisMontaj (a commercial package) was used for the inversion.

Acknowledgements

This work was funded by the Council for Geoscience, South Africa, statutory program and the U.S. Geological Survey Mineral Resources Program (United States). Any use of trade, firm, or product names is for descriptive purposes only and does not imply endorsement by the U.S. Government. We thank Dana Peterson and Lew Ashwal for helpful reviews of a draft of the manuscript and Eldridge Kgaswane for providing shear-wave velocity models. We extend our gratitude to the reviewers for their insightful comments, which contributed to the enhancement of our manuscript. There are no conflicts of interest.

Data Availability Statement.

The gravity data used for modelling and petrophysical and geological data constraining the models were collected by the Council for Geoscience and are publically available at https://maps.geocience.org.za. Registration is required. OasisMontaj, a commercial software package, was used for the inversion.

References

Alghamdi, A.H., Aitken, A.R., Dentith, M.C., 2018. The deep crustal structure of the Warakurna LIP, and insights on Proterozoic LIP processes and mineralisation. Gondw. Res. 56, 1–11. https://doi.org/10.1016/j.gr.2017.12.001.

Artemieva, I.M., Vinnik, L.P., 2016. Density structure of the cratonic mantle in Southern Africa: 2. Correlations with kimberlite distribution, seismic velocities, and Moho sharpness. Gondw. Res. 36, 14–27. https://doi.org/10.1016/j.gr.2016.05.002.

Ashwal, L.D., Webb, S.J., Knoper, M.W., 2005. Magmatic stratigraphy in the Bushveld Northern Lobe: continuous geophysical and mineralogical data from the 2950 m Bellevue drillcore. S. Afr. J. Geol. 108, 199–232. https://doi.org/10.2113/108.2.233.

Bedrosian, P.A., Peacock, J.R., Bowles-Martinez, E., Schultz, A., Hill, G.J., 2018. Crustal inheritance and a top-down control on arc magmatism at Mount St Helens. Nat. Geosci. 11, 865–870. https://doi.org/10.1038/s41561-018-0217-2.

Beukes, N.J., De Kock, M.O., Vorster, C., Ravhura, L.G., Frei, D., Gumsley, A.P., Harris, C., 2019. The age and country rock provenance of the Molopo Farms Complex: implications for Transvaal Supergroup correlation in southern Africa. S. Afr. J. Geol. 122, 39–56. https://doi.org/10.25131/sajg.122.0003.

Buchanan, D.L., 1975. The petrography of the Bushveld Complex intersected by boreholes in the Bethal area. Transactions of the Geological Society of South Africa 78, 335–348.

Campbell, G., 2011. Exploration geophysics of the Bushveld Complex in South Africa. The Leading Edge, June, 622–638. doi:10.1190/1.3599148.

Cashman, K.V., Sparks, R.S.J., Blundy, J.D., 2017. Vertically extensive and unstable magmatic systems: A unified view of igneous processes. Science 355, 1280. https://doi.org/10.1126/science.aag3055.

Cawthorn, R.G., 2007. Cr and Sr: Keys to parental magmas and processes in the Bushveld Complex, South Africa. Lithos 95, 381–398. https://doi.org/10.1016/j.lithos.2006.09.004.

Cawthorn, R.G., Walraven, F., 1998. Emplacement and Crystallization Time for the Bushveld Complex. J. Petrol. 39, 1669–1687. https://doi.org/10.1093/petroj/39.9.1669.

Chisenga, C., Jianguo, Y., Fadel, I., van der Meijde, M., Atekwana, E.A., 2020. Updated tectonic terrane boundaries of Botswana determined from gravity and aeromagnetic data. Episodes 43 (4), 919–933. https://doi.org/10.18814/EPIIUGS/2020/020054.

Christensen, N.I., 1996. Poisson's ratio and crustal seismology. J. Geophys. Res. 101, 3139–3156. https://doi.org/10.1029/95JB03446.

Christensen, N.I., Stanley, D., 2003. Seismic Velocities and Densities of Rocks, in International Handbook of Earthquake and Engineering Seismology. 81B, 1587–1593. https://doi.org/10.1016/S0074-6142(03)80278-4.

Clarke, B., Uken, R., Reinhardt, J., 2009. Structural and compositional constraints on the emplacement of the Bushveld Complex, South Africa. Lithos 111, 21–36. https://doi.org/10.1016/j.lithos.2008.11.006.

Cole, J., Webb, S.J., Finn, C.A., 2014. Gravity models of the Bushveld Complex - Have we come full circle? J. Afr. Earth Sc. 92, 97–118. https://doi.org/10.1016/j.jafrearsci.2014.01.012.

Cole, J., Finn, C.A., Webb, S.J., 2021. Geometry of the Bushveld Complex from 3D potential field modelling. Precambr. Res. 359, 106219 https://doi.org/10.1016/j.precamres.2021.106219.

Dankert, B.T., Hein, K.A.A., 2010. Evaluating the structural character and tectonic history of the Witwatersrand Basin. Precambr. Res. 177, 1–22. https://doi.org/10.1016/j.precamres.2009.10.007.

De Wit, M.J., Roering, C., Hart, R.J., Armstrong, R.A., De Ronde, C.E.J., Green, R.W.E., Tredoux, M., Peberdy, E., Hart, R.A., 1992. Formation of an Archaean continent. Nature 357, 553–562. https://doi.org/10.1038/357553a0.

Delph, J.R., Porter, R.C., 2015. Crustal structure beneath southern Africa: insight into how tectonic events affect the Mohorovicic discontinuity. Geophys. J. Int. 200, 254–264. https://doi.org/10.1093/gji/ggu376.

Du Plessis, C.P., Walraven, F., 1990. The tectonic setting of the Bushveld Complex in Southern Africa, Part 1. Structural Deformation and Distribution. Tectonophysics 179, 305–319. https://doi.org/10.1016/0040-1951(90)90296-K.

Durrheim, R.J., Green, R.W.E., 1992. A seismic refraction investigation of the Archaean Kaapvaal Craton, South Africa, using mine tremors as the energy source. Geophys. J. Int. 108, 812–832. https://doi.org/10.1111/j.1365-246X.1992.tb03472.x.

Eales, H.V., Costin, G., 2012. Crustally contaminated komatiite: Primary source of the chromitites and marginal, Lower, and Critical Zone magmas in a staging chamber beneath the Bushveld Complex. Econ. Geol. 107, 645–665. https://doi.org/10.2113/econgeo.107.4.645.

Fadel, I., van der Meijde, M., Paulssen, H., 2018. Crustal Structure and Dynamics of Botswana. J. Geophys. Res. Solid Earth 123, 10659–10671. https://doi.org/10.1029/2018JB016190.
Finn, C.A., Bedrosian, P.A., Cole, J.C., Khoza, T.D., Webb, S.J., 2015. Mapping the 3D extent of the Northern Lobe of the Bushveld layered mafic intrusion from geophysical data. Precambr. Res. 268, 279–294. https://doi.org/10.1016/j.precamres.2015.07.003.
Finn, C.A., Zientek, M.L., Parks, H.L., Peterson, D.E., 2020. Mapping the 3D extent of the Stillwater Complex, Montana—Implications for potential platinum group element exploration and development. Precambr. Res. 348, 105860 https://doi.org/10.1016/j.precamres.2020.105860.
Fouch, M.J., James, D.E., VanDecar, J.C., van der Lee, S., Kaapvaal Seismic Group, 2004. Mantle seismic structure beneath the Kaapvaal and Zimbabwe Cratons. S. Afr. J. Geol. 107, 33–44. https://doi.org/10.2113/107.1-2.33.
Geng, H., Brandl, G., Sun, M., Wong, J., Kröner, A., 2014. Zircon ages defining deposition of the Palaeoproterozoic Soutpansberg Group and further evidence for Eoarchaean crust in South Africa. Precambr. Res. 249, 247–262. https://doi.org/10.1016/j.precamres.2014.05.020.
Good, N., De Wit, M.J., 1997. The Thabazimbi-Murchison Lineament of the Kaapvaal Craton, South Africa: 2700 Ma of episodic deformation. J. Geol. Soc. London 154, 93–97. https://doi.org/10.1144/gsjgs.154.1.0093.
Gore, J., James, D.E., Zengeni, T.G., Gwavava, O., 2009. Crustal structure of the Zimbabwe Craton and the Limpopo Belt of Southern Africa: New constraints from seismic data and implications for its evolution. S. Afr. J. Geol. 112, 213–228. https://doi.org/10.2113/gssajg.112.3-4.213.
Hanski, E., Walker, R.J., Huhma, H., Suominen, I., 2001. The Os and Nd isotopic systematics of c. 2.44 Ga Akanvaara and Koitelainen mafic layered intrusions in northern Finland. Precambr. Res. 109, 73–102. https://doi.org/10.1016/S0301-9268(01)00142-5.
James, D.E., Niu, F., Rokosky, J., 2003. Crustal structure of the Kaapvaal craton and its significance for early crustal evolution. Lithos 71, 413–429. https://doi.org/10.1016/j.lithos.2003.07.009.
James, D.E., Fouch, M.J., VanDecar, J.C., van der Lee, S., Kaapvaal Seismic Group, 2001. Tectospheric structure beneath southern Africa. Geophys. Res. Lett. 28, 2485–2488. https://doi.org/10.1029/2000GL012578.
Jenkins, M.C., Mungall, J.E., Zientek, M.L., Costin, G., Yao, Z.-S., 2021. Origin of the J-M Reef and Lower Banded series, Stillwater Complex, Montana, USA. Precambr. Res. 367, 106457 https://doi.org/10.1016/j.precamres.2021.106457.
Jourdan, F., Féraud, G., Bertrand, H., Kampunzu, A.B., Tshoso, G., Watkeys, M.K., le Gall, B., 2005. Karoo large igneous province: Brevity, origin, and relation to mass extinction questioned by new 40Ar/39Ar age data. Geology 33, 745–748. https://doi.org/10.1130/G21632.1.
Kgaswane, E.M., Nyblade, A.A., Julià, J., Dirks, P.H.G.M., Durrheim, R.J., Pasyanos, M. E., 2009. Shear wave velocity structure of the lower crust in southern Africa: Evidence for compositional heterogeneity within Archaean and Proterozoic terrains. J. Geophys. Res. Solid Earth 114, 1–19. https://doi.org/10.1029/2008JB006217.
Kgaswane, E.M., Nyblade, A.A., Durrheim, R.J., Julià, J., Dirks, P.H.G.M., Webb, S.J., 2012. Shear wave velocity structure of the Bushveld Complex, South Africa. Tectonophysics 554–557, 83–104. https://doi.org/10.1016/j.tecto.2012.06.003.
Kruger, F.J., 2005. Filling the Bushveld Complex magma chamber: Lateral expansion, roof and floor interaction, magmatic unconformities, and the formation of giant chromitite, PGE and Ti-V-magnetitite deposits. Miner. Deposita 40, 451–472. https://doi.org/10.1007/s00126-005-0016-8.
Latypov, R., Chistyakova, S., 2022. Misinterpretation of zircon ages in layered intrusions. S. Afr. J. Geol. 125, 13–26. https://doi.org/10.25131/sajg.125.0001.
Latypov, R., Chistyakova, S., Barnes, S.J., Godel, B., Delaney, G.W., Cleary, P.W., Radermacher, V.J., Campbell, I., Jakata, K., 2022a. Chromitite layers indicate the existence of large, long-lived, and entirely molten magma chambers. Sci. Rep. 12, 4092. https://doi.org/10.1038/s41598-022-08110-6.
Latypov, R., Chistyakova, S., Hornsey, R.A., Costin, G., Van der Merwe, M., 2022b. A 5-km-thick reservoir with $> 380{,}000$ km^3 of magma within the ancient Earth's crust. Sci. Rep. 12, 15651. https://doi.org/10.1038/s41598-022-19915-w.
Maghdour-Mashhour, R., Hayes, B., Bolhar, R., Ueckermann, H., 2021. Sill intrusion into pyroxenitic mush and the development of the Lower-Upper Critical Zone boundary of the Bushveld Complex: Implications for the origin of stratiform anorthosites and chromitites in layered intrusions. J. Petrol. 62, egaa090. https://doi.org/10.1093/petrology/egaa090.
Maier, W.D., Barnes, S.J., Groves, D.I., 2013. The Bushveld Complex, South Africa: Formation of platinum-palladium, chrome- and vanadium-rich layers via hydrodynamic sorting of a mobilized cumulate slurry in a large, relatively slowly cooling, subsiding magma chamber. Miner. Deposita 48, 1–56. https://doi.org/10.1007/s00126-012-0436-1.
Mapeo, R.B.M., Kampunzu, A.B., Ramokate, L.V., Corfu, F., Key, R.M., 2004. Bushveld-age magmatism in southeastern Botswana: evidence from U-Pb zircon and titanite geochronology of the Moshaneng Complex. S. Afr. J. Geol. 107, 219–232. https://doi.org/10.2113/107.1-2.219.
Marsh, B.D., 2015. Magmatism, Magma, and Magma Chambers. In: Schubert, G. (Ed.), Treatise on Geophysics, Volume 1. Elsevier, pp. 275–333.
McDonald, I., Holwell, D.A., 2007. Did lower zone magma conduits store PGE-rich sulphides that were later supplied to the Platreef? S. Afr. J. Geol. 110, 611–616. https://doi.org/10.2113/gssajg.110.4.611.
Morelli, C., Gantar, C., Honkasalo, T., McConnel, R.K., Tanner, J.G., Szabo, B., Uotila, U., Whalen, C.T., 1974. The International Gravity Standardisation Net 1971 (IGSN71). Special Publication No. 4. International Association of Geodesy, Paris. Special Publication No. 4.
Moritz, H., 1992. Geodetic Reference System 1980. J. Geod. 66 (2), 128–133. https://doi.org/10.1007/BF00989270.
Mungall, J.E., Kamo, S.L., McQuade, S., 2016. U-Pb geochronology documents out-of-sequence emplacement of ultramafic layers in the Bushveld Igneous Complex of South Africa. Nat. Commun. 7, 13385. https://doi.org/10.1038/ncomms13385.
Nair, S.K., Gao, S.S., Liu, K.H., Silver, P.G., 2006. Southern African crustal evolution and composition: Constraints from receiver function studies. J. Geophys. Res. 111, B02304. https://doi.org/10.1029/2005JB003802.
Nguuri, T.K., Gore, J., James, D.E., Webb, S.J., Wright, C.I., Zengeni, T.G., Gwavava, O., Snoke, J.A., 2001. Crustal structure beneath southern Africa and its implications for the formation and evolution of the Kaapvaal and Zimbabwe cratons. Geophys. Res. Lett. 28, 2501–2504. https://doi.org/10.1029/2000GL012587.
Niu, F., James, D.E., 2002. Fine structure of the lowermost crust beneath the Kaapvaal craton and its implications for crustal formation and evolution. Earth Planet. Sci. Lett. 200, 121–130. https://doi.org/10.1016/S0012-821X(02)00584-8.
Odgers, A.T.R., Du Plessis, A., 1993. Interpretation of a regional reflection seismic survey in the north-eastern Bushveld Complex, In: 3rd Biennial Technical Meeting of the South African Geophysical Association, Cape Town, pp. 125–129.
Odgers, A.T.R., Hinds, R.C., Von Gruenewaldt, G., 1993. Interpretation of a seismic reflection survey across the southern Bushveld Complex. S. Afr. J. Geol. 96, 205–212.
Owen-Smith, T.M., Ashwal, L.D., 2015. Evidence for multiple pulses of crystal-bearing magma during emplacement of the Doros layered intrusion, Namibia. Lithos 238, 120–139. https://doi.org/10.1016/j.lithos.2015.08.019.
S. Özaydın K. Selway W.L. Griffin M. Moorkamp Probing the Southern African Lithosphere with Magnetotellurics: 2. Linking Electrical Conductivity, Composition, and Tectonomagmatic Evolution. Journal of Geophysical Research: Solid Earth 127 2022 e2021JB023105 10.1029/2021JB023105.
Parker, R.L., 1972. Inverse Theory with Grossly Inadequate Data. Geophys. J. R. Astron. Soc. 29, 123–138. https://doi.org/10.1111/j.1365-246X.1972.tb02203.x.
Peterson, D.E., Bedrosian. P., A., Finn, C.A., 2023. Subsurface characterization of the Duluth Complex and related intrusions from 3D modeling of gravity and magnetotelluric data, In: Institute on Lake Superior Geology. Proceedings-Part 1 – Program and Abstracts. Institute on Lake Superior Geology, Eau Claire, Wisconsin, pp. 63-64.
Prevec, S.A., Ashwal, L.D., Mkaza, M.S., 2005. Mineral disequilibrium in the Merensky Reef, western Bushveld Complex, South Africa: New Sm-Nd isotopic evidence. Contrib. Miner. Petrol. 149, 306–315. https://doi.org/10.1007/s00410-005-0650-2.
Roelofse, F., Ashwal, L.D., 2012. The lower Main Zone in the northern limb of the Bushveld Complex - a >1·3 km thick sequence of intruded and variably contaminated crystal mushes. J. Petrol. 53, 1449–1476. https://doi.org/10.1093/petrology/egs022.
Roelofse, F., Ashwal, L.D., Romer, R.L., 2015. Multiple, isotopically heterogeneous plagioclase populations in the Bushveld Complex suggest mush intrusion. Chem. Erde 75, 357–364. https://doi.org/10.1016/j.chemer.2015.07.001.
Schaller, M., Steiner, O., Studer, I., Holzer, L., Herwegh, M., Kramers, J.D., 1999. Exhumation of Limpopo Central Zone granulites and dextral continent-scale transcurrent movement at 2.0 Ga along the Palala Shear Zone, Northern Province. South Africa. Precambrian Research 96, 263–288. https://doi.org/10.1016/S0301-9268(99)00015-7.
Schulte-Pelkum, V., Mahan, K.H., Shen, W., Stachnik, J.C., 2017. The distribution and composition of high-velocity lower crust across the continental US: Comparison of seismic and xenolith data and implications for lithospheric dynamics and history. Tectonics 36, 1455–1496. https://doi.org/10.1002/2017TC004480.
Scoates, J.S., Wall, C.J., Friedman, R.M., Weis, D., Mathez, E.A., VanTongeren, J.A., 2021. Dating the Bushveld Complex: timing of crystallization, duration of magmatism, and cooling of the world's largest layered intrusion and related rocks. J. Petrol. 62, egaa107. https://doi.org/10.1093/petrology/egaa107.
Skursch, O., Corfu, F., Tegner, C., Lesher, C.E., Andreasen, R., Hagen-Peter, G., Vervoort, J.D., 2022. Zircon U-Pb chronology and Hf isotopes of the Lebowa Granite Suite and petrogenesis of the Bushveld Complex, South Africa. Contrib. Miner. Petrol. 177, 26. https://doi.org/10.1007/s00410-022-01889-7.
Sparks, R.S.J., Annen, C., Blundy, J.D., Cashman, K.V., Rust, A.C., Jackson, M.D., 2019. Formation and dynamics of magma reservoirs. Philos. Trans. R. Soc. A Math. Phys. Eng. Sci. 377, 20180019. https://doi.org/10.1098/rsta.2018.0019.
Stankiewicz, J., De Wit, M., 2013. 3.5 billion years of reshaped Moho, southern Africa. Tectonophysics 609, 675–689. https://doi.org/10.1016/j.tecto.2013.08.033.
Stettler, R.H., du Plessis, J.G., Hattingh, P.J., Venter, C.P., Hattingh, E., 2000. Regional gravity survey of the 2528 (Pretoria) 1:250 000 sheet. Council for Geoscience, Unpublished Report 2000-0043, 66 pp.
Tegner, C., Cawthorn, R.G., Kruger, F.J., 2006. Cyclicity in the main and upper zones of the Bushveld Complex, South Africa: Crystallization from a zoned magma sheet. J. Petrol. 47, 2257–2279. https://doi.org/10.1093/petrology/egl043.
Teigler, B., Eales, H. V, 1996. The Lower and Critical Zones of the western limb of the Bushveld Complex as intersected by the Nooitgedacht boreholes. Council for Geoscience, Bulletin 111, 126 pp.
Webb, S.J., Cawthorn, R.G., Nguuri, T., James, D., 2004. Gravity modeling of Bushveld Complex connectivity supported by Southern African Seismic Experiment results. S. Afr. J. Geol. 107, 207–218. https://doi.org/10.2113/107.1-2.207.
Wilding, J.D., Zhu, W., Ross, Z.E., Jackson, J.M., 2022. The magmatic web beneath Hawai'i. Science 379, 462–468. https://doi.org/10.1126/science.ade5755.
Wilson, A.H., 2012. A Chill Sequence to the Bushveld Complex: Insight into the First Stage of Emplacement and Implications for the Parental Magmas. J. Petrol. 53, 1123–1168. https://doi.org/10.1093/petrology/egs011.

Wilson, A.H., 2015. The earliest stages of emplacement of the eastern Bushveld Complex: Development of the Lower Zone, Marginal Zone and Basal Ultramafic Sequence. J. Petrol. 56, 347–388. https://doi.org/10.1093/petrology/egv003.

Yao, Z., Mungall, J.E., Jenkins, M.C., 2021. The Rustenburg Layered Suite formed as a stack of mush with transient magma chambers. Nat. Commun. 12, 505. https://doi.org/10.1038/s41467-020-20778-w.

Youssof, M., Thybo, H., Artemieva, I.M., Levander, A., 2013. Moho depth and crustal composition in Southern Africa. Tectonophysics 609, 267–287. https://doi.org/10.1016/j.tecto.2013.09.001.

Zandt, G., Ammon, C.J., 1995. Continental crust composition constrained by measurements of crustal Poisson's ratio. Nature 374, 152–154. https://doi.org/10.1038/374152a0.

Zeh, A., Ovtcharova, M., Wilson, A.H., Schaltegger, U., 2015. The Bushveld Complex was emplaced and cooled in less than one million years - results of zirconology, and geotectonic implications. Earth Planet. Sci. Lett. 418, 103–114. https://doi.org/10.1016/j.epsl.2015.02.035.

Zhu, L., Kanamori, H., 2000. Moho depth variation in southern California from teleseismic receiver functions. J. Geophys. Res. 105, 2969–2980. https://doi.org/10.1029/1999JB900322.